

# Numerical Simulation of Macroscopic Traffic Equations

Dirk Helbing and Martin Treiber

The increasing need for efficient traffic optimization measures is making reliable, fast, and robust methods for traffic simulation more and more important. Apart from the development of cellular automata models of traffic flow, this need has stimulated studies of suitable numerical algorithms for the solution of macroscopic traffic equations based on partial differential equations.<sup>1-9</sup>

The numerical integration of partial differential equations is a particularly difficult task, and there is no generally applicable method. In contrast to ordinary differential equations, the most natural explicit finite difference methods such as replacing differentials by forward, backward, or central finite differences often are numerically unstable,<sup>10,11</sup> even in the limit of very small discretizations in space and time. For example, a necessary condition for stability is that the maximum speed at which information about the solution can be propagated by the numerical method must be always greater than the propagation velocity of the exact solution.<sup>10,22</sup>

In general, the numerical solution of partial differential equations requires special methods, which work only under certain conditions.<sup>10,22</sup> Implicit integration methods are usually more stable, but they require the frequent solution of linear systems with multi-diagonal matrices. In this column, we will discuss only explicit methods, because they are useful for the varying boundary conditions found in realistic traffic simulations, where data is continuously fed into the simulation. In addition, explicit methods are more flexible for the simulation of on- and off-ramps or entire road networks.

## Macroscopic Traffic Models

Because the number of vehicles is conserved, all macroscopic traffic models are based on

---

Dirk Helbing and Martin Treiber are members of the II. Institute of Theoretical Physics, University of Stuttgart, Pfaffenwaldring 57, D-70550 Stuttgart, Germany.

the continuity equation for the vehicle density  $\rho(x, t)$  per lane at position  $x$  and time  $t$ :

$$\frac{\partial \rho}{\partial t} + \frac{\partial(\rho V)}{\partial x} = \pm \nu^\pm(x, t), \quad (1)$$

where  $V(x, t)$  is the average vehicle velocity. According to Eq. (1), the temporal change  $\partial\rho/\partial t$  of the vehicle density is given by the spatial change  $-\partial Q/\partial x$  of the traffic flow  $Q(x, t) = \rho(x, t)V(x, t)$  and the rate  $\nu^\pm(x, t) \geq 0$  of vehicles entering (+) or leaving (-) the highway at on- or off-ramps.

To describe time and spatially varying velocities such as occur in emergent traffic jams and stop-and-go traffic, we need a dynamical velocity equation. For most continuous models, this equation can be written as<sup>12</sup>

$$\frac{\partial V}{\partial t} + \underbrace{V \frac{\partial V}{\partial x}}_{\text{Transport Term}} = \underbrace{-\frac{1}{\rho} \frac{\partial P}{\partial x}}_{\text{Pressure Term}} + \underbrace{\frac{1}{\tau}(V_e - V)}_{\text{Relaxation Term}}. \quad (2)$$

According to Eq. (2), the change  $\partial V/\partial t$  of the average vehicle velocity is given by three terms. The transport term originates from the propagation of the velocity profile with the velocity  $V$  of the vehicles. The pressure term reflects either an anticipation of spatial changes in the traffic situation or dispersion effects due to a finite variance of the vehicle velocities. The relaxation term describes the adaptation to a dynamic equilibrium velocity  $V_e$  with a relaxation time  $\tau$ .

All forms of congested traffic seem to have almost universal properties which are largely independent of the initial conditions and the spatially averaged density. For example, the characteristic outflow  $Q_{\text{out}}$  from traffic jams is about  $1800 \pm 200$  vehicles per kilometer and lane, and a typical dissolution velocity  $C$  of about  $-15 \pm 5$  kilometers per hour.<sup>13</sup> This universality arises from the highly correlated state of motion produced by traffic congestions.<sup>14</sup> In particular, the outflow  $Q_{\text{out}}$  is related to the time interval between successive departures from the traffic jam. Therefore, the outflow is almost independent of the kind and density of congested traffic. As a consequence of the constant outflow, the dissolution velocity of traffic jams is nearly constant as well. These observations and the transition from free to

“synchronized” congested traffic<sup>15</sup> are correctly described by the nonlocal, gas-kinetic-based traffic model,<sup>16–19</sup> which we now introduce.

### The Nonlocal, Gas-Kinetic-Based Traffic Model

Our approach is to derive macroscopic traffic models from gas-kinetic traffic equations,<sup>12,16</sup> which are obtained from “microscopic” models of driver-vehicle behavior.<sup>16</sup> Gas-kinetic traffic models have been proposed earlier, but the correct treatment of the most interesting regime of moderate and high densities was still an open problem.

We have managed to evaluate the vehicular interaction term of the gas-kinetic traffic model almost exactly.<sup>16</sup> The analytical result can be represented by the nonlocal, dynamical equilibrium velocity  $V_e$ :

$$V_e = V_0 \left[ 1 - \frac{\theta + \theta'}{2A(\rho_{\max})} \left( \frac{\rho' T}{1 - \rho'/\rho_{\max}} \right)^2 B(\delta_V) \right]. \quad (3)$$

According to Eq. (3),  $V_e$  is given by the desired (maximum) velocity  $V_0$ , reduced by a term which reflects necessary deceleration maneuvers. Here,  $\rho_{\max}$  is the maximum vehicle density, and  $T$  is the average time headway at large densities. For example, German authorities require that the distance in meters to the front vehicle be not less than half the velocity in km per hour, which gives a time headway of  $T = 1.8$  s. For the intra-lane variance  $\theta$ , we assume the constitutive relation  $\theta = A(\rho)V^2$  where  $A(\rho)$  is given by Eq. (5). The prime indicates that the variable is calculated at the advanced “interaction point”  $x' = x + \gamma(1/\rho_{\max} + VT)$  with  $1 \leq \gamma < 2$  rather than at the actual position  $x$ . This factor accounts for the fact that drivers anticipate the behavior of vehicles in front of them. The monotonically increasing “Boltzmann factor”

$$B(\delta_V) = 2 \left[ \delta_V \frac{e^{-\delta_V^2/2}}{\sqrt{2\pi}} + (1 + \delta_V^2) \int_{-\infty}^{\delta_V} dy \frac{e^{-y^2/2}}{\sqrt{2\pi}} \right] \quad (4)$$

describes<sup>16</sup> the dependence of the braking interaction on the dimensionless velocity difference  $\delta_V = (V - V')/\sqrt{\theta + \theta'}$  between the actual location  $x$  and  $x'$ . In homogeneous traffic, we have  $B(0) = 1$ . If the preceding cars are much slower ( $\delta_V \gg 0$ ), the interaction strength

given by  $B$  is particularly large, and it follows that  $B(\delta_V) = 2\delta_V^2$ . For  $\delta_V \ll 0$ , we have  $B(\delta_V) \approx 0$ . That is, because the distance to the next vehicle is increasing, the vehicle will not brake, even if its distance is smaller than the safe distance.

Finally, the dynamics of the intra-lane variance can be approximated by the constitutive relation

$$\theta(x, t) = A(\rho)V^2(x, t) = \left[ A_0 + \Delta A \tanh\left(\frac{\rho(x, t) - \rho_c}{\Delta\rho}\right) \right] V^2(x, t), \quad (5)$$

where the coefficients  $A_0 = 0.008$ ,  $\Delta A = 0.02$ ,  $\rho_c = 0.27\rho_{\max}$ , and  $\Delta\rho = 0.05\rho_{\max}$  have been obtained from single-vehicle data on a section of the Dutch motorway A9.<sup>16</sup> Simulations of sections of other motorways, for example, the German motorway A8, give a somewhat lower value of  $\Delta A = 0.01$ , which we will use in the following. Equation (5) shows that the standard deviation  $\sqrt{\theta}$  of vehicle velocities is proportional to the average velocity  $V$ , with a density-dependent proportionality factor which is small for the density range found in free traffic. The velocity variance also enters the gas-kinetic traffic pressure

$$P(x, t) = \rho(x, t)\theta(x, t). \quad (6)$$

If not explicitly stated otherwise, the simulation results presented here were calculated with the model parameters  $V_0 = 110$  km/h,  $\tau = 32$  s,  $T = 1.8$  s,  $\rho_{\max} = 160$  vehicles/km, and  $\gamma = 1.2$ .

The main difference between the gas-kinetic-based traffic model and other macroscopic traffic models is the nonlocal character of the braking term. The nonlocal term in Eq. (3) has smoothing properties similar to those of a viscosity term, but its effect is forwardly directed and, therefore, more realistic. In contrast, models with an explicit viscosity term<sup>20</sup> lead to unphysical humps in the vehicle density (see Figure 1) and even negative velocities<sup>21</sup> (see Figure 2). Our model also has favorable properties with respect to numerical stability and integration speed, and hence allows a robust real time simulation of freeway stretches up to several thousand kilometers on a personal computer.

## Some Explicit Finite Difference Methods

A desirable property of the above traffic equations is that they can be formulated in terms of a conservation equation with a sink/source term  $\mathbf{s}$ :

$$\frac{\partial \mathbf{u}}{\partial t} + \frac{\partial \mathbf{f}(\mathbf{u})}{\partial x} = \mathbf{s}(\mathbf{u}). \quad (7)$$

This form makes it possible to use a variety of numerical standard methods developed for the simulation of hydrodynamic problems.<sup>10,11,22</sup> The conservative form of the traffic equations reads

$$\frac{\partial \rho}{\partial t} + \frac{\partial Q}{\partial x} = \pm \nu^\pm(x, t), \quad (8)$$

and

$$\frac{\partial Q}{\partial t} + \frac{\partial (Q^2/\rho + P)}{\partial x} = \frac{\rho V_e - Q}{\tau} \pm \nu^\pm V^\pm, \quad (9)$$

where  $Q(x, t) = \rho(x, t)V(x, t)$  is the traffic flow and  $V^\pm$  denotes the average velocity of vehicles which enter (+) or leave (-) the freeway at ramps. For the case  $V^\pm \neq V$ , we obtain the additional terms  $\pm \nu^\pm(V^\pm - V)/\rho$  in (2). We have

$$\mathbf{u} = [\rho, Q], \quad (10)$$

$$\mathbf{f} = [Q, (Q^2/\rho + P)], \quad (11)$$

$$\mathbf{s} = [\pm \nu^\pm, (\rho V_e - Q)/\tau \pm \nu^\pm V^\pm]. \quad (12)$$

For the explicit numerical solution methods we will discuss,  $x$  and  $t$  are discretized with uniform values of  $\Delta x$  and  $\Delta t$ , respectively. Hence, we calculate  $\mathbf{u}$  at the discrete points  $(j \Delta x, n \Delta t)$  with  $j, n \in \{0, 1, 2, \dots\}$ . For brevity, we use the notation  $\mathbf{u}_j^n = \mathbf{u}(j \Delta x, n \Delta t)$ . We will discuss the following numerical integration methods:<sup>10,22</sup>

### 1. Lax-Friedrichs method

$$\mathbf{u}_j^{n+1} = \frac{\mathbf{u}_{j-1}^n + \mathbf{u}_{j+1}^n}{2} - \frac{\Delta t}{2\Delta x}(\mathbf{f}_{j+1}^n - \mathbf{f}_{j-1}^n) + \Delta t \mathbf{s}_j^n. \quad (13)$$

### 2. Upwind method

$$\mathbf{u}_j^{n+1} = \mathbf{u}_j^n - \frac{\Delta t}{\Delta x}(\mathbf{f}_j^n - \mathbf{f}_{j-1}^n) + \Delta t \mathbf{s}_j^n. \quad (14)$$

### 3. MacCormack method

$$\tilde{\mathbf{u}}_j^n = \mathbf{u}_j^n - \frac{\Delta t}{\Delta x}(\mathbf{f}_j^n - \mathbf{f}_{j-1}^n) + \Delta t \mathbf{s}_j^n, \quad (\text{predictor}) \quad (15)$$

$$\mathbf{u}_j^{n+1} = \frac{1}{2} \left[ \tilde{\mathbf{u}}_j^n + \mathbf{u}_j^n - \frac{\Delta t}{\Delta x}(\tilde{\mathbf{f}}_{j+1}^n - \tilde{\mathbf{f}}_j^n) + \Delta t \tilde{\mathbf{s}}_j^n \right]. \quad (\text{corrector}) \quad (16)$$

### 4. Lax-Wendroff method

$$\mathbf{u}_{j+\frac{1}{2}}^{n+\frac{1}{2}} = \frac{1}{2} \left[ \mathbf{u}_j^n + \mathbf{u}_{j+1}^n - \frac{\Delta t}{\Delta x}(\mathbf{f}_{j+1}^n - \mathbf{f}_j^n) + \frac{\Delta t}{2}(\mathbf{s}_j^n + \mathbf{s}_{j+1}^n) \right] \quad (\text{predictor}) \quad (17)$$

$$\mathbf{u}_j^{n+1} = \mathbf{u}_j^n - \frac{\Delta t}{\Delta x}[\mathbf{f}_{j+\frac{1}{2}}^{n+\frac{1}{2}} - \mathbf{f}_{j-\frac{1}{2}}^{n+\frac{1}{2}}] + \frac{\Delta t}{2}[\mathbf{s}_{j+\frac{1}{2}}^{n+\frac{1}{2}} + \mathbf{s}_{j-\frac{1}{2}}^{n+\frac{1}{2}}]. \quad (\text{corrector}) \quad (18)$$

*Consistency Order.* If the spatial variation of  $\mathbf{u}$  is sufficiently smooth, the Lax-Friedrichs and upwind methods are first-order, that is, the upper bound of the local error is proportional to  $\alpha$  if  $\Delta x$  and  $\Delta t$  are simultaneously decreased by a factor of  $\alpha$ . In general, the upwind method is not stable and the differential operator needs to be decomposed into parts which are treated by upwind and downwind differencing, respectively (the Godunov method<sup>22,5-7</sup>). Fortunately, for traffic equations of the form (2), the upwind method is stable (and equivalent to the Godunov method).

The two-step MacCormack and Lax-Wendroff methods are second-order, that is, the upper bound of the local error is proportional to  $\alpha^2$ . However, for shock-like solutions, the order is lower for all of the above integration methods.<sup>22</sup> Note that the predictor step of the MacCormack method is an ordinary upwind step, and the corrector step consists of the average between the predictor and a “downwind” step with  $\mathbf{f}$  calculated with the values of the predictor. Interchanging the order of the upwind and downwind differencings of the two steps has nearly no effect for the equations investigated here.

*Accuracy.* Although the discretization errors associated with nonlinear equations are difficult to determine, good estimates are usually obtained by doing a local linearization, at least for smooth solutions.<sup>22</sup> Because realistic traffic models can produce sharp gradients, but

no real shock fronts, the linearization is applicable to the numerical treatment of macroscopic traffic equations. This analysis shows that the upwind method is more accurate than the Lax-Friedrichs method.

Although the main discretization error of the Lax-Friedrich and upwind methods yields a numerical diffusion, which causes a smoothening of shock fronts (see Figures 3a, and (b)), for the MacCormack and Lax-Wendroff methods there is numerical dispersion, which is associated with a slower propagation of waves with small amplitudes and can lead to oscillations in the density and flow fields behind (but not before) large gradients (cf. Figures 3c and (d)). However, nonlinear instabilities (see below) also may lead to oscillations. An example is the oscillations at the downstream front of the large amplitude jam of Figure 3d.

*Numerical Stability.* An integration method is numerically unstable if errors grow exponentially, which usually leads to wildly oscillating density profiles with very short wave lengths and eventually to overflow error. Even in the quasi-linear case, the above explicit discretization methods can lead to three types of instabilities which implies three conditions for numerical stability:

1. *Convective instability.* Instabilities of the finite difference method for the flux term lead to the Courant-Friedrichs-Lewy condition<sup>10,22</sup> which for our model becomes

$$|\Delta t| \leq \frac{\Delta x}{V_0}, \quad (19)$$

where  $V_0$  is the maximum average velocity. For example, for  $V_0 = 40$  m/s (144 km/h) and a spatial discretization of  $\Delta x = 20$  m, we obtain  $\Delta t \leq 0.5$  s.

2. *Diffusion instability.* Models which contain an explicit viscosity term  $D\partial^2 V/\partial x^2$ , change the otherwise hyperbolic character of the partial differential equations to a parabolic one. For numerical stability, the additional diffusional Courant-Friedrichs-Lewy condition  $D(\Delta x)^2/(2\Delta t) \leq 1$  must be fulfilled.<sup>10,22</sup> This condition does not apply to simulations of the nonlocal, gas-kinetic-based traffic model.

3. *Relaxational instability.* Due to the finite  $\Delta t$ , instabilities can develop for spatially homogeneous density and flow fields if  $\Delta t$  is larger than one of the local relaxation times  $1/r_k$ , where  $r_k$  are the eigenvalues of the functional matrix of the sink/source term  $\mathbf{s}$ . This condition puts further restrictions on  $\Delta t$ , which depend on the maximum vehicle density in the simulation.

Because viscosity and diffusion terms are replaced by a nonlocal term, coarser discretization is possible in the above gas-kinetic-based traffic model than in most other traffic models, allowing real time simulation of much larger systems. For simulations of this model, good results are obtained for  $\Delta x = 20$  m and  $\Delta t = 0.4$  s for the MacCormack as well as the upwind method. Figure 4 shows that a finer discretization gives almost identical results.

The development of traffic instabilities starting with almost homogeneous initial traffic is a very strict test of numerical accuracy (see Figure 4). In most situations, for example, when simulating fronts or already developed congested traffic, the accumulated discretization error is much smaller.

In addition to the quasi-linear instabilities discussed above, genuine nonlinear instabilities may arise for certain numerical methods and simulation conditions. An example is the oscillations at the downstream front of the large amplitude jam of Figure 3d. It turns out that second-order methods are more sensitive to these instabilities. Note that, although the quasi-linear behavior is the same for the MacCormack and Lax-Wendroff methods, the nonlinear behavior can be different.<sup>10</sup> For the above traffic equations, *the MacCormack method is more stable than the Lax-Wendroff method*, and hence we will use the MacCormack method whenever a second-order method is desired.

When simulating the nonlocal model with one of the first-order methods, we did not observe nonlinear instabilities. Furthermore, *higher order methods are not necessarily more accurate*,<sup>11</sup> especially for large gradients. Thus, one should always implement different numerical methods and compare their simulation results. Aside from their double integration speed, it is sometimes preferable to use first-order methods (causing somewhat smoothed

wave fronts) instead of second-order methods (producing oscillations and sometimes non-linear numerical instabilities). One reason is that oscillations act like perturbations, which may give rise to additional traffic jams that do not correspond with reality.

### Initial and Boundary Conditions

To calculate traffic flows, it is necessary to specify the initial and boundary conditions. The initial conditions are completely determined by specifying  $\mathbf{u}(x, 0)$  in a range  $[0, L + \delta]$ , where  $L$  is the length of the simulated section and  $\delta$  is the maximum nonlocality, which is of the order of 30 m in the gas-kinetic-based model. In systems with open rather than periodic boundaries, the initial conditions usually influence the simulation results only for a short time, at least, if we start with free traffic, because errors in the specification of the initial conditions are propagated outside the simulated freeway stretch very quickly. Thus, the choice of the initial conditions is unimportant. For example, we can start with a linear interpolation of the measured initial boundary values. However, because of conservation of vehicle number, the initial conditions are relevant for closed systems with *periodic boundary conditions*, which are given by  $\mathbf{u}(0, t) = \mathbf{u}(L, t)$ , and  $\partial\mathbf{u}(0, t)/\partial x = \partial\mathbf{u}(L, t)/\partial x$ .

The specification of time-dependent boundary conditions is much more involved. The following options are reasonable in different situations:

1. *Dirichlet boundary conditions* are given by the empirically measured values  $\mathbf{u}(0, t)$  and  $\mathbf{u}(L, t)$  at both ends of the particular freeway stretch. For the values at  $x \in [L, L + \delta]$  beyond the right boundary (required by the nonlocal term of the gas-kinetic-based model), a constant  $\mathbf{u}(x) = \mathbf{u}(L)$  of the boundary values is assumed.
2. *Homogeneous von Neumann boundary conditions* assume that the density and vehicular flow remain unchanged at the boundaries  $x = 0$  and  $x = L$ :

$$\frac{\partial\mathbf{u}(0, t)}{\partial x} = 0, \quad \frac{\partial\mathbf{u}(L, t)}{\partial x} = 0. \quad (20)$$

Again, a constant value of  $\mathbf{u}$  is assumed for  $x > L$ .

3. *Free boundary conditions* assume that the traffic state is smooth at the boundary,

$$\frac{\partial^2 \mathbf{u}(0, t)}{\partial x^2} = \frac{\partial^2 \mathbf{u}(L, t)}{\partial x^2} = 0, \quad (21)$$

with a linear extrapolation  $\mathbf{u}(L + \delta x) = \mathbf{u}(L) + \delta x \partial \mathbf{u}(L) / \partial x$  for  $\delta x \in [0, \delta]$ .

4. *In- and outflows*  $\pm Q_{\text{rmp}}$  at on-ramps (+) and off-ramps (-), can be considered as follows.<sup>17–19</sup> If  $n$  is the number of freeway lanes (without ramps) and  $L_{\text{rmp}}$  is the length of the ramp, we simply set

$$\nu^\pm = \frac{Q_{\text{rmp}}}{nL_{\text{rmp}}}. \quad (22)$$

Generally speaking, periodic boundary conditions are best suited for theoretical investigations of stability, and Dirichlet boundary conditions are best for simulations of real traffic with measured values of velocity and the traffic flow at the boundary. Homogeneous von Neumann or free boundary conditions for “absorbing” boundaries should be used if the traffic situation outside the boundaries is not of interest. The effects of the latter two boundary conditions are nearly the same. An alternative to using open boundaries is to apply periodic boundary conditions for distances which are much longer than the freeway stretch of interest. However, for a simulated time interval  $T_{\text{sim}} = 2$  h, the required additional length is order  $V_0 T_{\text{sim}} \approx 200$  km, which considerably reduces the efficiency of the numerical integration.

There are problems associated with using Dirichlet boundary conditions. Imposing Dirichlet boundary conditions at both sides usually leads to an overdetermined system, so that either numerical instabilities occur or the boundary conditions are simply ignored by the integration method. Even Dirichlet boundary conditions at one of the two boundaries will lead to an unphysical, ill-posed problem in certain situations. This case becomes clear when imposing downstream Dirichlet boundary conditions for free traffic flow at low densities. If the imposed boundary flow is higher than the flow arriving from the simulated section at the boundary, the continuity equation will lead to a decrease of the density, which

eventually results in unphysical negative densities. On the other hand, if Dirichlet boundary conditions are imposed at the upstream boundary in a situation of congested traffic where the boundary flow is higher than the equilibrium flow, the continuity equation leads to an increased density implying an even lower equilibrium flow. This positive feedback will eventually lead to a divergence of the density near the boundary.

We solve this problem by dynamically switching between Dirichlet and von Neumann boundary conditions, depending on the density close to the boundaries. The idea is to use Dirichlet boundary conditions if the direction of information flow points towards the simulation stretch, and von Neumann boundary conditions otherwise. Because the traffic equations contain source terms like the relaxation term, the propagation direction of information cannot be obtained from the characteristic velocities (which are the propagation velocities of locally linearized homogeneous partial differential equations like conservation equations without source terms). Rather, the linearized group velocity  $v_g = \partial Q_e / \partial \rho$  of kinematic waves gives a good criterion for separating the traffic situation into free traffic ( $v_g > 0$ ) whose information flow points downstream, and congested traffic ( $v_g < 0$ ) where the information flow points upstream. Based on this idea, the following hybrid boundary conditions yield good results: If the upstream boundary values  $\rho_0(t)$  and  $Q_0(t)$  satisfy

$$\rho_0(t) \leq \beta_1 \rho_m \quad \text{or} \quad Q_0(t) < \beta_2 Q(\Delta x, t) \quad (23)$$

Dirichlet boundary conditions are used;  $\rho_m$  is the density associated with maximum equilibrium flow,  $\beta_1 = 0.95$ , and  $\beta_2 = 0.98$ . Otherwise, homogeneous Von-Neumann boundary conditions are applied. For the downstream boundary conditions, the directions of the inequalities are exchanged. Note that these boundary conditions include situations where Dirichlet boundary conditions are necessary at both sides (for example, when a jam enters the downstream boundary of the simulation region) as well as situations where no Dirichlet boundary conditions are allowed at all (when congested traffic formed at an inhomogeneity within the simulated region reaches the upstream boundary).

We illustrate the effects of different boundary conditions by a simulation of the German

motorway A8 near Munich with real traffic data using the upwind method. Figure 5a shows a space-time plot of the density with Dirichlet boundary conditions on both sides. The wing-like regions of higher density represent “synchronized” congested traffic<sup>15</sup> forming upstream of a flow-reducing inhomogeneity,<sup>19</sup> while the region of the highest density represents a traffic jam entering through the downstream boundary. Note that the unnecessary downstream boundary conditions for  $t < 17:30$  h are ignored by the upwind differencing, whereas the traffic jam entering the downstream boundary for  $17:30 \text{ h} < t < 18:20 \text{ h}$  is accepted. This desirable behavior cannot be expected in general. For example, the MacCormack method is unstable in this situation.

Figure 5b demonstrates the remarkable property that the boundary conditions for the density are nearly irrelevant. Although the boundary conditions for the flow are the same as in Fig. 5a, a constant amount of 20 vehicles/km has been added artificially to the upstream boundary conditions for the density. Nevertheless, the traffic dynamics, in particular the spontaneous breakdown at  $x \approx 40$  km and  $t \approx 17:00$  h, is nearly unchanged. This behavior can be explained by recognizing that the inflow into the freeway and the outflow from it determine the number of vehicles on the freeway stretch, which cannot be changed by the traffic dynamics between the boundaries. Hence, changes of the traffic flow are far reaching, while the influence of density (or velocity) boundary conditions is restricted to the distance that the vehicles drive during the relaxation time.

Figure 5c illustrates the effect of using homogeneous von Neumann downstream boundary conditions instead of Dirichlet boundary conditions. For  $t < 18:00$  h, the situation is identical to Figure 5a. For  $t > 18:00$  h, however, the upstream moving traffic jam passing the downstream boundary is ignored. Hence, the simulation result is very different when the direction of the downstream information flow changes.

Finally, Fig. 5d shows a simulation with the hybrid boundary conditions (see Eq. (23)) and the upstream boundary shifted downstream by 3.5 km. In this case, the traffic jam reaches the upstream boundary, which is handled by the hybrid boundary conditions, while

all other boundary conditions would lead to a numerical instability for any integration method.

## Summary

We have seen that traffic flows are characterized by the occurrence of congested regions, jams, and stop-and-go waves which are associated with large gradients of the vehicle density and average velocity. This rich behavior has stimulated an intense research activity. We have discussed the problems of macroscopic traffic simulations which are related to the numerical integration of systems of coupled nonlinear partial differential equations. Despite the differences with hydrodynamic equations, many integration methods developed for conservation equations turn out to be applicable. Compared to implicit methods,<sup>10</sup> explicit methods are less robust, but much more flexible with regard to time-dependent boundary conditions and (variational) optimization problems, and are usually computationally faster. Among the explicit first-order methods, the upwind method is more accurate than the Lax-Friedrichs method. The MacCormack and the two-step Lax-Wendroff methods are second-order, but they are less efficient by a factor of two and produce unrealistic oscillations close to steep gradients. The numerical precision may be improved by “high resolution methods,”<sup>22</sup> where a first-order method is used for large gradients and a second-order method is used for small gradients. This approach may combine the accuracy of the second-order methods with the smoothness of the first-order methods.

The most important factor that determines the computation time is the choice of the traffic model. In particular, the simulation of the nonlocal, gas-kinetic-based traffic model is significantly more efficient than the numerical solution of models with viscosity or diffusion terms. This efficiency is mainly related to the fact that the diffusional Courant-Friedrichs-Lewy condition, which does not apply for nonlocal terms, is usually far more restrictive than the other instability conditions, especially for fine discretizations. Because diffusion terms also produce unrealistic effects close to steep gradients, it may be reasonable to generally replace models with diffusion or viscosity terms by nonlocal models. Anyway, diffusion and

viscosity terms are often a lowest-order approximation of nonlocal terms. They are mainly used for historical reasons, because they can be better treated analytically.

Finally, we have discussed suitable specifications of the boundary conditions. In most previous simulation studies, periodic boundary conditions were used to circumvent the intricate problems related to open boundaries, which are required for the simulation of real freeways. We found that Dirichlet boundary conditions work in some cases, but fail in others, because of overspecification. The most successful treatment is based on hybrid boundary conditions which switch between Dirichlet and homogeneous von Neumann (or free) boundary conditions depending on the respective direction of information flow.

### Acknowledgments

The authors are grateful for financial support by the DFG (Heisenberg scholarship He 2789/1-1) and by the BMBF (research project SANDY, grant No. 13N7092). D. H. also thanks Tamas Vicsek for his warm hospitality at the Institute of Biological Physics, where part of this column was written.

### Suggestions for Further Study

1. *Parameter-dependence of flow-density relation.* (a) Find the density dependence of the stationary, homogeneous solution for the average velocity  $V_e$  in the nonlocal, gas-kinetic-based traffic model by setting the temporal and spatial derivatives to zero and solving for  $V$ . (b) The flow-density relation  $Q_e(\rho) = \rho V_e(\rho)$  depend on which of the model parameters,  $V_0$ ,  $\tau$ ,  $\gamma$ ,  $T$ , and  $\rho_{\max}$ ? Which parameters are irrelevant for the stationary homogeneous solution? (c) Plot  $Q_e$  and the velocity-density relation  $V_e$  for different parameter sets. Start with the values used in this column. Check that a speed limit (that is, a decrease in  $V_0$ ) reduces the flow at small densities, but only by a negligible amount for medium and high densities. In addition, compare pure car traffic with  $V_0 = 130$  km/h,  $T = 1.2$  s, and  $\rho_{\max} = 160$  vehicles/km with traffic containing a considerable fraction of trucks with, for example,  $V_0 = 90$  km/h,  $T = 3$  s, and  $\rho_{\max} = 110$  vehicles/km. In which density regimes do the flow-density relations almost agree, and in which are they very different?<sup>16,18</sup>

2. *Stability of homogeneous traffic with respect to a localized perturbation.* Simulate freeway traffic for a circular road of 10 km circumference with the nonlocal, gas-kinetic-based traffic model and the parameters used in this column. Assume homogeneous equilibrium traffic of density  $\bar{\rho}$ , and add to the density a localized perturbation of amplitude  $\Delta\rho$  so that the initial conditions are given by<sup>23</sup>

$$\begin{aligned}\rho(x, 0) &= \bar{\rho} + \Delta\rho \left[ \cosh^{-2} \left( \frac{x - x_0}{w^+} \right) - \frac{w^+}{w^-} \cosh^{-2} \left( \frac{x - x_0 - \Delta x_0}{w^-} \right) \right], \\ Q(x, 0) &= Q_e(\bar{\rho}).\end{aligned}$$

Here,  $x_0$  and  $x_0 + \Delta x_0$  are the positions of the positive and negative peaks of the perturbation with widths  $w^+$  and  $w^-$ , respectively. Choose  $w^+ = 200$  m,  $w^- = 800$  m, and  $\Delta x_0 = w^+ + w^- = 1000$  m. Use linear interpolation to calculate the nonlocal terms and take into account that the circular road implies that  $\mathbf{u}(L + \delta x) = \mathbf{u}(\delta x)$ . Perform the simulations with the upwind method on a fixed grid with spatial and temporal discretizations of  $\Delta x = 20$  m and  $\Delta t = 0.4$  s.

(a) Choose a small perturbation amplitude of  $\Delta\rho = 1$  vehicle/km and run the simulation for 30 minutes. Check that the perturbation does not grow for  $\bar{\rho} < \rho_{c2}$  and  $\bar{\rho} > \rho_{c3}$  with  $\rho_{c2} = 29$  vehicles/km and  $\rho_{c3} = 47$  vehicles/km, but gives rise to large-amplitude stop-and-go waves for  $\rho_{c2} \leq \bar{\rho} \leq \rho_{c3}$ .

(b) Use larger perturbations of amplitudes up to  $\Delta\rho = 60$  vehicles/km and show the traffic flow is metastable. To do so, show that the model produces a single traffic jam for  $\bar{\rho} \in (\rho_{c1}, \rho_{c2})$  with  $\rho_{c1} = 27$  vehicles/km and a dipole-like localized structure for  $\bar{\rho} \in (\rho_{c3}, \rho_{c4})$  with  $\rho_{c4} = 50$  vehicles/km, if  $\Delta\rho$  exceeds a (density-dependent) critical amplitude; homogeneous traffic flow is found for subcritical perturbation amplitudes.<sup>23,16</sup>

(c) In sufficiently large systems, there exists a subset of densities  $\bar{\rho} \in (\rho_{cv}, \rho_{c3})$  in the linearly unstable regime where traffic is convectively stable.<sup>19</sup> This stability means that the localized perturbation will disappear for  $t \rightarrow \infty$  at any given location  $x$  while, nevertheless, the global maximum of the perturbation grows (because the system is linearly unstable). In

our case,  $\rho_{cv}$  is given by the value of  $\bar{\rho}$  at which the downstream boundary of the perturbed zone does not move. Illustrate the case of convective stability by making a three-dimensional plot of  $\rho(x, t)$  of a simulation running for 15 minutes with  $\bar{\rho} = 45$  vehicles/km and  $\Delta\rho = 1$  vehicles/km. Show that  $\rho_{cv} = 42.5$  vehicles/km.

3. *Characteristic parameters.*<sup>16</sup> Assume a circular road, model parameters, and initial conditions as in Problem 2.

(a) Evaluate the densities of fully developed traffic jams and of free traffic at the outflows of jams. Determine the associated flows and the propagation velocity of jam fronts. Hint: To obtain the densities and flows, run the simulation for 60 minutes and analyze the fields  $\rho(x, t)$  and  $Q(x, t)$ . The jam density (density of free traffic) is simply the global maximum (minimum) of the density, and the jam flow (outflow from jams) is the global minimum (maximum) of the flows. To obtain the group velocity, save the density as a function of time at a given position (for example,  $x = 10$  km) and determine the time intervals needed for the jams to propagate around the circular road. Use the last interval to avoid effects of transients.

(b) Plot the densities, the flows, and the propagation velocity in separate plots as a function of the average density  $\bar{\rho}$  for a perturbation amplitude  $\Delta\rho = 10$  vehicle/km. What do you find? Check that there is a density range in which the density inside and outside of traffic jams, the associated flows, and the propagation velocity are independent of  $\bar{\rho}$ , so that these quantities are characteristic parameters of traffic flows.

(c) Show numerically that the traffic inside and outside of jams is nearly in equilibrium. Also show that the group velocity can be expressed analytically in terms of the densities and flows inside and outside of jams. This relation means that only two of the characteristic parameters, for example, the group velocity and the outflow from jams, are independent quantities.

(d) Do Problems 2a, 2b, and 3a for different values of the relaxation time  $\tau$ . Show that with increasing  $\tau$ , the region of linearly unstable traffic and the regions of metastable

traffic and the jam density increase, while the outflow from jams decreases. In particular, homogeneous traffic is always stable for  $\tau \leq 18$  s.

4. *“Synchronized” congested traffic.*<sup>17</sup> This traffic state occurs if a perturbation reaches a stationary inhomogeneity of the road which can be an on-ramp for example.

(a) Simulate a freeway of length 10 km with open boundaries and an on-ramp of length  $L_{\text{rmp}} = 400$  m at  $x_{\text{rmp}} = 5$  km by assuming in Eqs. (8) and (9) a source term  $\nu^+ = Q_{\text{rmp}}/L$  inside the ramp region  $x \in [x_{\text{rmp}} - L/2, x_{\text{rmp}} + L/2]$ , but  $\nu^+ = 0$  otherwise. Assume  $\tau = 40$  s, the usual values for the other model parameters, and homogeneous equilibrium traffic of density  $\bar{\rho} = 15$  vehicles/km without perturbations as initial conditions. To obtain stationary conditions, simulate the first 20 minutes with a constant ramp flow  $Q_{\text{rmp}} = 500$  vehicles/h using homogeneous von Neumann boundary conditions at both sides of the road. Now, introduce a perturbation of amplitude  $\Delta Q_{\text{rmp}} = 150$  vehicles/km by linearly increasing the ramp flow up to  $Q_{\text{rmp}} + \Delta Q_{\text{rmp}}$  at  $t = 22.5$  min, and decreasing it again to  $Q_{\text{rmp}}$  at  $t = 25$  min. After running the simulation for a total of 60 minutes, you should see “synchronized” congested traffic, that is, an increasing region of high density and low velocity, but relatively high flow, whose upstream front is propagating upstream, while the downstream front is pinned at the ramp.

(b) Verify that “synchronized” congested traffic is in equilibrium and determine the numerical value of its outflow  $\tilde{Q}_{\text{out}}$ . Show that the propagation velocity  $v_g$  of the upstream front can be expressed by the relation

$$v_g = \frac{\tilde{Q}_{\text{out}} - Q_{\text{rmp}} - Q_{\text{main}}}{\rho_{\text{cong}}(\tilde{Q}_{\text{out}} - Q_{\text{rmp}}) - \rho_{\text{free}}(Q_{\text{main}})},$$

where  $Q_{\text{rmp}}$  and  $Q_{\text{main}} = Q_e(\bar{\rho})$  are the inflows at the ramp and to the main road. The densities  $\rho_{\text{cong}}(Q)$  and  $\rho_{\text{free}}(Q)$  denote, in accordance with  $Q_e = \rho V_e(\rho)$ , congested traffic ( $\rho \geq 31$  vehicles/km) and free traffic ( $\rho < 31$  vehicles/km), respectively.

5. *Different traffic states close to an on-ramp.*<sup>19</sup> Varying the initial traffic density, the length of the on-ramp, and the ramp flow leads to several interesting states of congested

traffic. Do simulations as in Problem 4 with (a)  $\bar{\rho} = 20$  vehicles/km,  $Q_{\text{rmp}} = 250$  vehicles/h,  $\Delta Q_{\text{rmp}} = 150$  vehicles/km, (b)  $\bar{\rho} = 20$  vehicles/km,  $Q_{\text{rmp}} = 150$  vehicles/h,  $\Delta Q_{\text{rmp}} = 150$  vehicles/km, and (c)  $\bar{\rho} = 17$  vehicles/km,  $Q_{\text{rmp}} = 250$  vehicles/h,  $\Delta Q_{\text{rmp}} = 550$  vehicles/km. You should observe (a) oscillating congested traffic, (b) triggered stop-and-go waves, and (c) pinned localized congestion. By varying the inflow  $Q_{\text{main}} = Q_e(\bar{\rho})$  to the main road, verify that oscillating congested traffic emerges, if the expression for  $v_g$  in Problem 4 is negative (upstream moving front); otherwise pinned localized congestion or free traffic occur.

## REFERENCES

- <sup>1</sup> C. F. Daganzo, “A finite difference approximation of the kinematic wave model of traffic flow,” *Transportation Research B* **29**(4), 261–276 (1995).
- <sup>2</sup> C. J. Leo and R. L. Pretty, “Numerical simulation of macroscopic continuum traffic models,” *Transportation Research B* **26**, 207–220 (1992).
- <sup>3</sup> P. G. Michalopoulos, D. E. Beskos, and J.-K. Lin, “Analysis of interrupted traffic flow by finite difference methods,” *Transportation Research B* **18**, 409–421 (1984).
- <sup>4</sup> P. G. Michalopoulos, P. Yi, and A. S. Lyrintzis, “Continuum modelling of traffic dynamics for congested freeways,” *Transportation Research B* **27**, 315–332 (1993).
- <sup>5</sup> J. P. Lebacque, *The Godunov Scheme and What it Means for First Order Traffic Flow Models* (Centre d’Enseignement et de Recherche en Mathématique, Informatique et Calcul Scientifique, ENPC, La Courtine, F-NOISY-LE-GRAND Cedex, 1995).
- <sup>6</sup> R. Ansorge, “What does the entropy condition mean in traffic flow theory?,” *Transportation Research B* **24**, 133–143 (1990).
- <sup>7</sup> D. D. Bui, P. Nelson, and S. L. Narasimhan, “Computational Realizations of the Entropy Condition in Modeling Congested Traffic Flow.” Report No. FHWA/TX-92/1232-7, Texas A&M University, April 1992.
- <sup>8</sup> P. S. Babcock IV, D. M. Auslander, M. Tomizuka, and A. D. May, “Role of adaptive discretization in a freeway simulation model,” *Transportation Research Record* **971**, 80–92 (1984).
- <sup>9</sup> W. Kronjäger and P. Konhäuser, “Applied Traffic Flow Simulation,” in *Transportation Systems*, edited by M. Papageorgiou and A. Pouliezios (International Federation of Automatic Control, Chania, Greece, 1997), Vol. II, pp. 805–808.
- <sup>10</sup> D. A. Anderson, J. C. Tannehill, and R. H. Pletcher, *Computational Fluid Mechanics and*

*Heat Transfer* (Hemisphere Publishing Corporation, N.Y., 1984).

- <sup>11</sup> W. H. Press, S. A. Teukolsky, W. T. Vetterling, and B. P. Flannery, *Numerical Recipes in C: The Art of Scientific Computing* (Cambridge University Press, Cambridge, 2nd edition, 1992).
- <sup>12</sup> D. Helbing, “Derivation and empirical validation of a refined traffic flow model,” *Physica A* **233**, 253–282 (1996).
- <sup>13</sup> B. S. Kerner and H. Rehborn, “Experimental features and characteristics of traffic jams,” *Phys. Rev. E* **53**, R1297–R1300 (1996).
- <sup>14</sup> B. S. Kerner, “Experimental characteristics of traffic flow for evaluation of traffic modelling,” in *Transportation Systems*, edited by M. Papageorgiou and A. Pouliezios (International Federation of Automatic Control, Chania, Greece, 1997), Vol. II, pp. 793–798.
- <sup>15</sup> B. S. Kerner and H. Rehborn, “Experimental properties of phase transitions in traffic flow,” *Phys. Rev. Lett.* **79**, 4030–4033 (1997).
- <sup>16</sup> M. Treiber, A. Hennecke, and D. Helbing, “Derivation, properties, and simulation of a gas-kinetic-based, non-local traffic model,” *Phys. Rev. E* **59**, 239–253 (1999).
- <sup>17</sup> D. Helbing and M. Treiber, “Gas-kinetic-based model explaining observed hysteretic phase transition,” *Phys. Rev. Lett.* **81**, 3042–3045 (1998).
- <sup>18</sup> M. Treiber and D. Helbing, “Macroscopic simulation of widely scattered synchronized traffic states,” *J. Phys. A: Math. Gen.* **32**, L17–L23 (1999).
- <sup>19</sup> D. Helbing, A. Hennecke, and M. Treiber, “Phase diagram of traffic states in the presence of inhomogeneities,” preprint cond-mat/9809324, *Phys. Rev. Lett.*, in print (1999).
- <sup>20</sup> H. Y. Lee, H. W. Lee, and D. Kim, “Origin of synchronized traffic flow on highways and its dynamic phase transition,” *Phys. Rev. Lett.* **81**, 1130–1133 (1998).
- <sup>21</sup> C. F. Daganzo, “Requiem for second-order fluid approximations of traffic flow,” *Trans-*

portation Research B **29**(4), 277–286 (1995).

<sup>22</sup> R. J. LeVeque, *Numerical Methods for Conservation Laws* (Birkhäuser, Basel, 1992).

<sup>23</sup> B. S. Kerner and P. Konhäuser, “Structure and parameters of clusters in traffic flow,”  
Phys. Rev. E **50**, 54–83 (1994).

## FIGURES

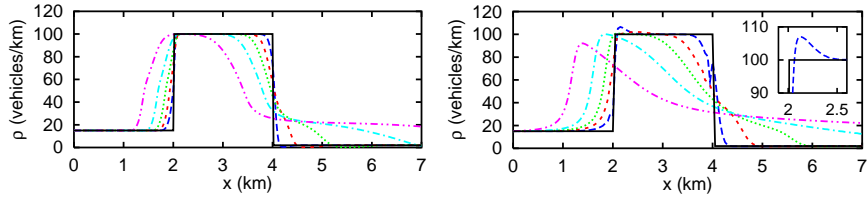


FIG. 1. Simulation of discontinuous initial conditions for (a) the non-local, gas-kinetic-based traffic model, and (b) for a typical traffic model with a viscosity term.<sup>20</sup> The density profile is shown at  $t = 0$  s (—), 10 s (— —), 30 s (- - -), 60 s (· · ·), 120 s (- · -), and 240 s (- · ·). The inset of (b) shows an unrealistic detail of the profile (upstream front) at  $t = 10$  s. Also note that, in (b), the upstream front propagates too fast.

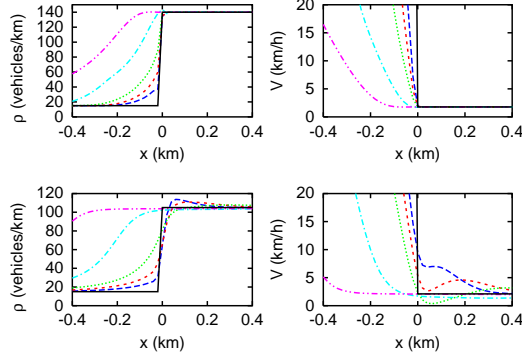


FIG. 2. First stages of the density and velocity profiles evolving from a discontinuous upstream front (solid lines) corresponding, for example, to an end of a traffic jam behind a curve. The lines correspond to  $t = 0$  s (—), 5 s (---), 10 s (- - -), 20 s (⋯), 60 s (- · -), and 120 s (- · ·). Parts (a) and (b) show simulations with the non-local, gas-kinetic-based model ( $\Delta x = 20$  m,  $\Delta t = 0.1$  s), while (c) and (d) correspond to a typical traffic model with a viscosity term.<sup>20</sup> To obtain comparable equilibrium velocities in the initial jam, the initial jam densities  $\rho_{\text{jam}}^{(a/b)} = 140$  vehicles/h and  $\rho_{\text{jam}}^{(c/d)} = 105$  vehicles/h were chosen differently. In the viscosity traffic model, the finite velocity diffusion leads to an increase of velocity also in the congested part (see (d)) and to a subsequent further increase of density (see (c)). The ensuing positive density gradient would lead to negative velocities for an initial jam density higher than 106 vehicles/km, which is much lower than the maximum density  $\rho_{\text{max}} = 160$  vehicles/km.

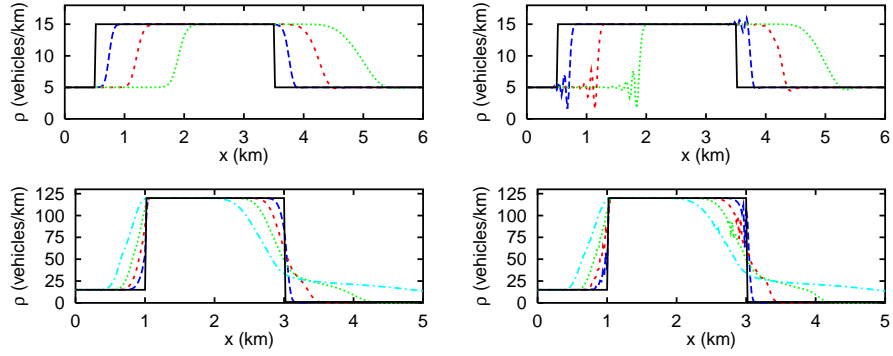


FIG. 3. Comparison of the upwind method, (a) and (c), with the MacCormack method, (b) and (d), for simulations of the nonlocal, gas-kinetic-based traffic model with discontinuous initial conditions (—). The plots correspond to transitions between free traffic at two different vehicle densities (see (a) and (b)), and to transitions to and from congested traffic with backwards propagating fronts (see (c) and (d)). The density is shown at  $t = 0$  s (—), 10 s (---), 30 s (- - -), 60 s ( $\cdot\cdot\cdot$ ), and 120 s ( $- \cdot -$ ) (only in (c) and (d)). In the MacCormack method simulations, the oscillations behind the large gradient result from the dispersion error (see (b)), whereas the oscillations around  $x = 3$  km originate from nonlinear instabilities (see (d)).

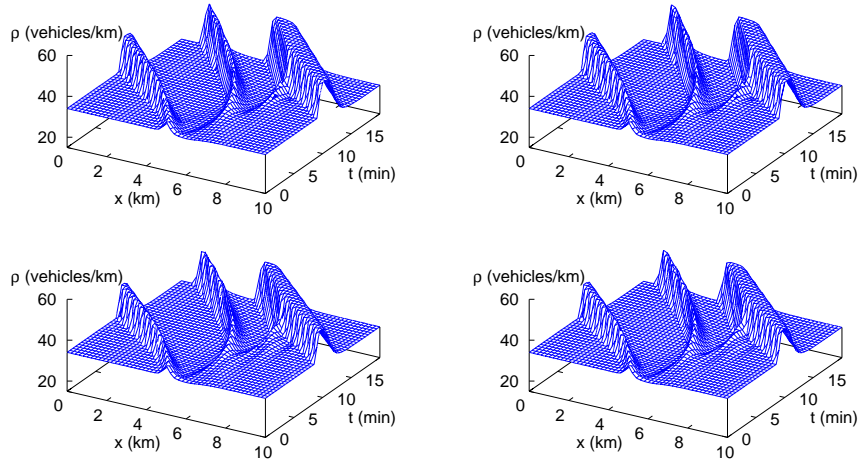


FIG. 4. Spatio-temporal formation of stop-and-go waves, simulated with the non-local, gas-kinetic-based traffic model, using different integration methods and discretizations. (a) MacCormack method with  $\Delta t = 0.4$  s and  $\Delta x = 20$  m. (b) Upwind method with  $\Delta t = 0.4$  s and  $\Delta x = 20$  m. (c) Upwind method with  $\Delta t = 0.01$  s and  $\Delta x = 20$  m. (d) Upwind method with  $\Delta t = 0.1$  s and  $\Delta x = 5$  m.

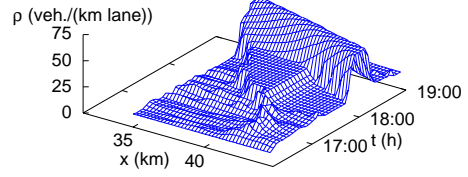
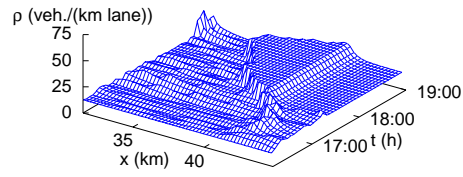
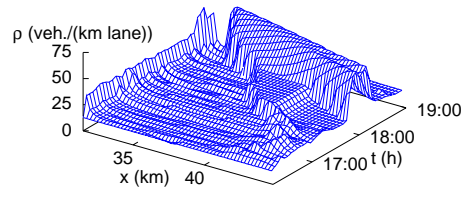
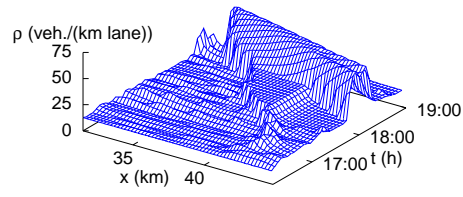


FIG. 5. Simulation with empirical boundary conditions at the German freeway A8 near Munich. with the model parameters  $V_0 = 130$  km/h for  $x \leq 41$  km,  $V_0 = 97$  km/h for  $x > 41$  km,  $\tau = 32$  s,  $T = 2.0$  s,  $\rho_{\max} = 110$  vehicles/km, and  $\gamma = 1.2$ ,  $A_0 = 0.008$ ,  $\Delta A = 0.01$ ,  $\rho_c = 0.27\rho_{\max}$ , and  $\Delta\rho = 0.1\rho_{\max}$ . Note that the decreased desired velocity for  $x > 41$  km reflects a flow-reducing gradient on the freeway stretch. (a) Dirichlet boundary conditions, applied to  $\rho$  and  $Q$  at the upstream and downstream boundaries. We can distinguish two different kinds of congestion: a region of “synchronized” traffic<sup>17,19</sup> with increased homogeneous density, and a backwards propagating traffic jam entering the freeway stretch at the downstream boundary. Dirichlet boundary conditions are applicable here, because the traffic jam does not reach the upstream boundary. (The jam dissolves before, as the inflow decreases in the course of time.) (b) As in (a), but with a constant  $\Delta\rho = 20$  vehicles/km added to the measured density at the upstream boundary. The congested traffic enforced at the boundary relaxes to free traffic very quickly. Note that the downstream traffic patterns do not change significantly, because the boundary flows (and, hence, the number of entering and leaving vehicles per time unit) are the same as in (a). Nevertheless, this result suggests that the congested traffic patterns are self-organized structures. (c) As in (a), but with homogeneous von Neumann boundary conditions for flow and density at the downstream boundary, which ignore the upstream moving traffic jam entering at the downstream boundary. However, the homogeneous congested region of “synchronized” traffic is correctly reproduced, which indicates that it is not triggered by the downstream boundary condition, but it is rather generated by the inflow to the motorway at the upstream boundary together with the flow-reducing gradient beginning at  $x = 41.0$  km. (d) Simulation with the hybrid boundary conditions (23). Compared to (a), we shifted the upstream boundary by 3.5 km in downstream direction, so that it is reached by the jam. The resulting spatio-temporal traffic patterns are nearly identical as in (a), indicating that the hybrid boundary conditions handle dynamically emerging congestion in a natural way, even at the boundaries.